CSIRO PUBLISHING

www.publish.csiro.au/journals/ajc

Aust. J. Chem. **2011**, *64*, 617–624

Disordered Mesoporous Gadolinosilicate Nanoparticles Prepared Using Gadolinium Based Ionic Liquid Emulsions: Potential as Magnetic Resonance Imaging Contrast Agents

Guozhen Liu,[A] *Nicholas M. K. Tse,*[A,B] *Matthew R. Hill,*[A] *Danielle F. Kennedy,*[A] *and Calum J. Drummond*[A,C]

[A]CSIRO Materials Science and Engineering (CMSE), Private Bag 10, Clayton South MDC, Vic. 3169, Australia.

[B]Particulate Fluids Processing Centre, School of Chemistry, The University of Melbourne, Melbourne, Vic. 3010, Australia.

[C]Corresponding author. Email: calum.drummond@csiro.au

Gadolinium doped mesoporous silica (gadolinosilicate) nanoparticles were synthesized using a novel approach aimed at incorporating Gd ions into a porous silica network. The ionic liquid, gadolinium (*Z*)-octadec-9-enoate (Gd Oleate) was utilized in a dual role, as a soft template to generate porous silica and also to act as a gadolinium source for incorporation into the silicate. The generated silicate materials were characterized for size, structure and composition, confirming that gadolinium was successfully doped into the silicate network in a mesoporous nanoparticulate form. Proton relaxivity results indicated that the gadolinium doped silicates had slightly lower longitudinal relaxivity and much higher transverse relaxivity than the commercial contrast agent Magnevist®, suggesting that the mesoporous nanoparticulate materials have potential as contrast agents for magnetic resonance imaging.

Manuscript received: 7 February 2011.
Manuscript accepted: 12 April 2011.

Introduction

Magnetic resonance imaging (MRI) is a commonly used medical diagnostic technique. Its role in medical research and preventive health-care is rapidly evolving.[1] This non-invasive technique is used to map the physiological structures of biological systems. MRI distinguishes between different tissue types based on their water environment.[1–3] However, there are many situations where the contrast between adjacent tissues is not strong enough to allow clear distinctions to be made, or to enable the observation of fine structures. This has prompted the development of a new class of non-therapeutic diagnostic compounds known as contrast agents (CAs). CAs frequently incorporate a paramagnetic metal, which modifies the nuclear relaxation of surrounding protons, for example Gd chelates and iron oxides.[4] CAs are used to enhance images by improving the contrast between areas containing the contrast agent and adjacent tissues. CAs are used clinically in a variety of diagnostic applications, such as targeted drug delivery systems (DDSs),[5,6] cell labelling[7] and angiography,[8] with up to 30% of MRI screenings performed in conjunction with the administration of contrast agent.[9]

A CA provides image contrast by shortening both the longitudinal (T_1) and transverse (T_2) relaxation times. The potency of a CA can be directly compared by the longitudinal (R_1) and transverse (R_2) relaxivity values, which are calculated based on the inverse of the relaxation time ($1/T_1$) and ($1/T_2$) versus the concentration of contrast agent. An effective MRI contrast agent will have a relatively large relaxivity value, R_1 (positive CA) or R_2 (negative CA).

An effective CA must possess several features including, a strong effect on proton relaxation of water, water stability, low toxicity and high dispersibility in biological fluids and be smaller than 150 nm in diameter.[10] According to the standard Solomon-Bloembergen-Morgan (SMB) treatment,[11,12] there are several factors that influence the efficiency of a CA including: the duration and exchange rate of water molecules with inner sphere water around a paramagnetic centre, the rate of water exchanges in the outer water sphere and the average molecular (or particle) tumbling of the paramagnetic ion.[9,13] Commonly used CAs are paramagnetic small metallochelate agents, which have been developed since the 1980s; detailed reviews of this field have been published by Caravan et al.[9,13,14]

The lanthanide ion, gadolinium or Gd^{III}, is the most commonly used paramagnetic ion, because of its large magnetic moment with a long electron spin relaxation time.[15] Free Gd^{III} ions are highly toxic. Therefore Gd^{III} ions are conventionally sequestered by chelation[13] or encapsulation[16,17] in order to reduce toxicity. However, these techniques reduce the number of water molecules coordinated to Gd^{III} ions, resulting in compromised effectiveness. Commercial CAs are dominated by highly stable gadolinium complexes based on the polyaminocarboxylate ligand, e.g. $[Gd(DTPA)(H_2O)]^{2-}$ (gadolinium(III) diethylene triamine pentaacetate hydrate).[18] However, these small molecule CAs are non-specific, and lack the required image contrast ability.[1,2,8,19–21] In rare instances, Gd-DTPA small molecules and derivatives have been the cause of nephrogenic systemic fibrosis (NSF), a condition in which

 10.1071/CH11064 0004-9425/11/050617

tissues are thickened, hence these diagnostic agents are contra-indicated for patients with either acute kidney injury (AKI) or chronic kidney disease (CKD).[22,23] The drive in the development of new types of contrast agents are therefore to achieve a lower toxicity and an increased contrast ability.[1,2] Various attempts aiming to increase the sensitivity and improve the selective localization of CAs have been made by developing efficient nanoparticulate carrier systems.[24]

Mesoporous silica nanoparticles have many attractive features, such as stable mesoporous structures forming networks of channels, large surface areas, tuneable pore sizes and volumes.[25] As optically transparent, biocompatible, and low toxicity materials, this makes them ideal for the hosting of molecules over a wide range of sizes, shapes, and functionalities.[26] In addition, the surface of silica particles can be easily modified to attach biomolecules such as proteins, antibodies, peptides or oligonucleotides of interest for cell-specific targeting and delivery.[27] The porous nature of the network of channels in mesoporous silica nanoparticles permits the movement of water molecules and at the same time maintains the rigidity of the frame, thus offering a strong and penetrable matrix for water exchange. Nanosized porous silica would be an excellent carrier for Gd^{III} ions for the development of contrast agents for magnetic resonance imaging. Lin et al. have reported the preparation of Gd loaded nanosized mesoporous silica using a long-chain surfactant as a template.[28] These Gd loaded silica nanoparticles can have significantly higher r_1 and r_2 relaxivities than $[Gd(DTPA)(H_2O)]^{2-}$.

Recently we reported the synthesis and investigation of a novel class of metal containing oleate ionic liquids.[29] Neat gadolinium (*Z*)-octadec-9-enoate (Gd Oleate) was found to melt to an ionic liquid at 37°C.

Herein we report a new approach to synthesize Gd doped silica using a protic ionic liquid, Gd oleate, as a template to produce a potential MRI contrast agent. Such synthesized Gd^{III} doped mesoporous silica has an average particle size of 100 nm and disorderedly arranged pores with an average pore diameter of 2.5 nm. The synthesized mesoporous nanoparticles were found to be monodisperse, and were characterized with a range of analytical techniques to determine their size, structure and elemental composition. Proton relaxivity was also studied to evaluate the potential of these materials as an MRI contrast agent.

Experimental

Unless stated otherwise, all chemicals were used as received, without further purification. Tetraethyl orthosilicate (TEOS), cetyltrimethylammonium bromide (CTAB), sodium hydroxide, and 1-pentanol (99.9%), gadolinium chloride hexahydrate (99%) were all obtained from Sigma-Aldrich. Oleic acid (99% purity) was obtained from Fluka.

Synthesis of MCM-41 Type Silica Samples

The control silica samples were synthesized according to the method reported by Cai et al.[30] A typical preparation of MCM-41 type sample is as following: 1.0 g of CTAB was dissolved in 470 mL of Milli-Q water, 3.5 mL of 2 M NaOH solution and 10 mL 1-pentanol. The solution was then heated to 80°C and homogenized by stir agitation. After complete dissolution, 5 mL of TEOS was added dropwise to give a white slurry. The solution was then stirred for 48 h, the resulting product was collected by centrifugation, washed with Milli-Q water, and freeze-dried overnight. The samples collected were then calcined in air at 550°C for 4 h to remove the templates. The final product is a white powder.

Synthesis of Gd-doped Silica Samples

The Gd doped sample was made in a similar fashion as the MCM-41 type silica. The templating surfactant CTAB was replaced by gadolinium oleate, which was synthesized according to Liu et al.[29] Different amounts of Gd doping were controlled by the amount of gadolinium oleate added. A list of synthetic composition values are tabulated in Table 1.

Characterization of Samples

X-ray powder diffraction (XRD) was undertaken on a Bruker D8 Advance X-ray diffractometer with CuKα radiation (40 kV, 40 mA) fitted with a graphite monochromator. Each sample was scanned over the 2θ range 1 to 62° with a step size of 0.02° and a count time of 4 s per step. Analyses were performed on the collected XRD data for each sample using the Bruker XRD search match program EVA™. Crystalline phases were identified using the ICDD-JCPDS powder diffraction database. X-ray photoelectron spectroscopy (XPS) analysis was performed using an AXIS-HSi spectrometer (Kratos Analytical Inc., Manchester, UK) with a monochromated Al K_α source at a power of 144 W (12 kV × 12 mA), a hemispherical analyzer operating in the fixed analyzer transmission mode and the standard aperture (1 × 0.5 mm). The total pressure in the main vacuum chamber during analysis was of the order of 10^{-8} mbar. Each specimen was analyzed at an emission angle of 0° as measured from the surface normal. A circular area with a diameter of ~1 mm was analyzed on each sample. All elements

Table 1. Synthetic composition values and measured particle size, specific surface area and pore size distribution for the silicate samples

Sample	CTAB [g]	Gd oleate [g]	Intended doping [wt%]	Particle size [nm][A]	BET surface area [$m^2 g^{-1}$][B]	Mean pore size [nm][C]	Total pore volume [$cm^3 g^{-1}$][D]
MCM-41	1	–	0	150	960	3.5	0.868
GdSi_A	–	0.26	3	148	172	7.5	0.330
GdSi_B	–	0.80	9	147	141	11.4	0.400
GdSi_C	–	1.00	12	75	150	8.0	0.387
GdSi_D	–	1.20	15	100	170	4.4	0.188
GdSi_E	–	2.00	18	110	144	8.5	0.217

[A]Determined from SEM micrographs.
[B]Determined from the adsorption branch of the N_2 isotherm using the BJH method.
[C]The PDS was calculated form the absorption branch of the N_2 isotherm.
[D]Measured at $P/P_o = 0.995$.

present were identified from survey spectra (acquired at a pass energy of 320 eV). High-resolution spectra were recorded from individual peaks at 40 eV pass energy. The atomic concentrations of the detected elements were calculated using integral peak intensities and the sensitivity factors supplied by the manufacturer.

The amount of gadolinium in the product was determined using a Varian Vista inductively coupled plasma atomic emission spectroscopy (ICP-AES).

Fourier transfer infrared spectroscopy (FT-IR) was performed using a BOMEN MB 101 from Extech Equipment Pty Ltd Spectra of the crystalline samples as KBr pellets were obtained at room temperature in the 4000–400 cm^{-1} range and were accumulated for 32 scans at a resolution of 8 cm^{-1}. Solid state ^{29}Si magic angle spinning (MAS) NMR spectra were recorded at 79.46 MHz, using a Bruker Advance 400 spectrometer. Sample morphology and microstructure were examined by Philips XL30 field emission scanning electron microscopy (FE-SEM). The accelerating voltage used was 2 kV.

The nitrogen adsorption-desorption experiments were performed on a Quantachrome Autosorb 1 at 77 K over the partial pressure range $0.005 < P/P_o < 0.975$. Prior to analysis, samples were degassed at 200°C and 5×10^{-3} Torr for 24 h. Specific surface area values were obtained using the Brunauer-Emmett-Teller (BET) equation and pore sizes by the Barrett-Joyner-Halenda (BJH) method.[31] Parameters including BET surface area, total pore volume, and BJH pore size distribution were determined using the 'Autosorb 1 for Windows' version 1.55 Software, © 2001.

The longitudinal and transverse relaxation time, T_1 and T_2, were measured at 20 MHz (0.47 T) with a MINISPEC from Bruker at 25°C in MQ water. For T_1 measurements, the standard inversion-recovery (IR) method was used as the pulse sequence. The recycle delay time was set to five times the T_1 value. Typically 20 points were taken for each T_1 measurement. For T_2 measurements, the Carr-Pucell-Meiboom-Gill (CPMG) method was used.[32] The longitudinal relaxivity and transverse relaxivity were then determined from the slope of the linear regression fits of $1/T_1$ and $1/T_2$ as a function of the Gd concentration, respectively.

Results

The various templated mesoporous silica materials synthesized according to the above methodology were characterized by using a range of techniques. Using scanning electron microscopy (SEM), the particle size, morphology and aggregation were analyzed for both the silica reference sample, MCM-41, and representative gadolinium doped samples. Fig. 1 shows SEM micrographs of a MCM-41 sample and a representative sample templated with Gd oleate, GdSi_C. The particles were found to be spherical in shape with an average particle size of 150 and 80 nm for MCM-41 and GdSi_C, respectively. The SEM also showed small degrees of particle aggregation for MCM-41.

XRD was used to investigate the porous structure of the two synthesized silica samples, as shown in Fig. 2. The pores of MCM-41 were found to be arranged in an ordered two dimensional (2D) hexagonal array, consistent with previous reports.[30] The four Bragg peaks with a d-spacing of 36.39, 21.40, 18.71 and 14.14 Å were indexed as the (100), (110), (200) and (210) reflections of the P6 mm space group, respectively. For the Gd-doped samples (e.g. GdSi_C in Fig. 2b) the diffractograms showed no distinguishable sharp peaks at lower two-theta. A broad peak at ~21° ($d \approx 4.2$ Å), indicates that the silica sample is amorphous in nature. The lack of sharp Bragg peaks suggests that any templated pores are disordered in the Gd-doped silica samples. Such disordered porosity may have been due to the weak interaction between the anionic inorganic species, silicate acid, and the templating agent, Gd oleate. The existence of porosity demonstrates that weak interaction between the two species exists. The lack of ordering of these pores in the final product is therefore a matter of reorganization between the Si^{4+}–Gd oleate emulsions within the solution.[33] Reorganization of emulsions could be impaired by the availability of hydrolyzed silicate acid. This suggests that silica species are partially condensed during the reorganization of the Si^{4+}–Gd oleate emulsions, thus restricting realignment of the emulsions. Further work will be performed to elucidate this proposal.

Using the nitrogen gas sorption technique, the surface area and the porosity were determined for all the synthesized silica based samples. Representative N_2 adsorption-desorption isotherms are shown in Fig. 3 and a summary of the pore size distribution (PSD), particle size and total pore volume is provided in Table 1. The MCM-41 reference sample exhibits a typical IV isotherm,[34] with a large hysteresis, indicating that it is highly mesoporous, whereas for the Gd doped silica samples, the lack of a sharp defined starting point of the hysteresis suggest that the pore size range is not narrowly defined. The

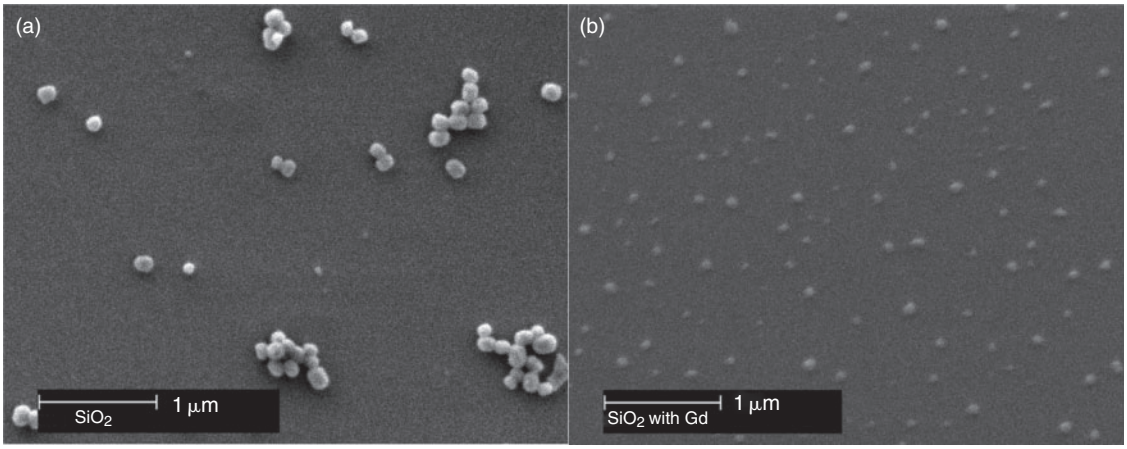

Fig. 1. Representative SEM micrographs of (a) MCM-41 and (b) GdSi_C samples.

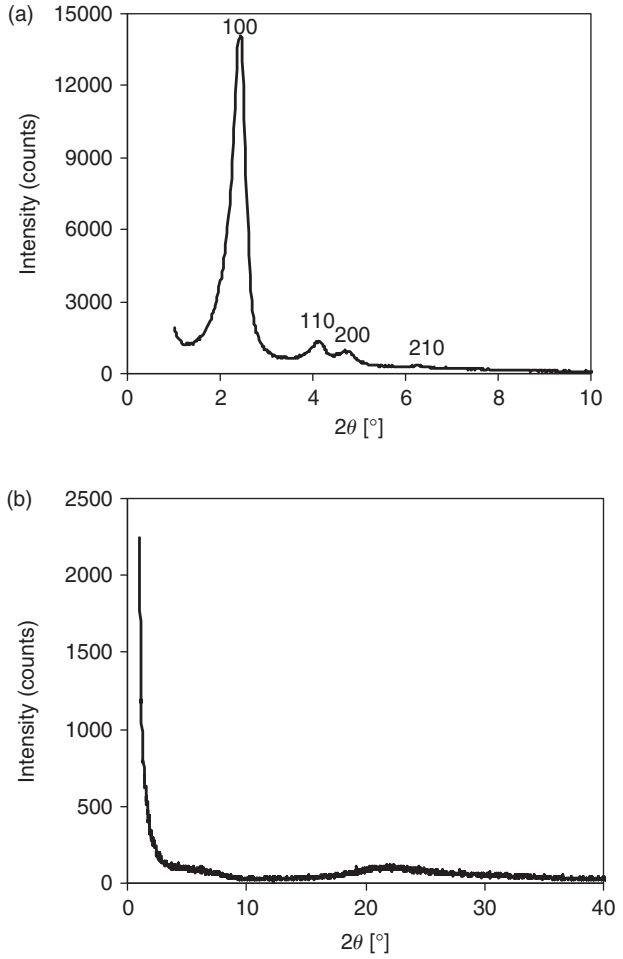

Fig. 2. Representative powder X-ray diffraction patterns for (a) MCM-41 and (b) GdSi_C samples.

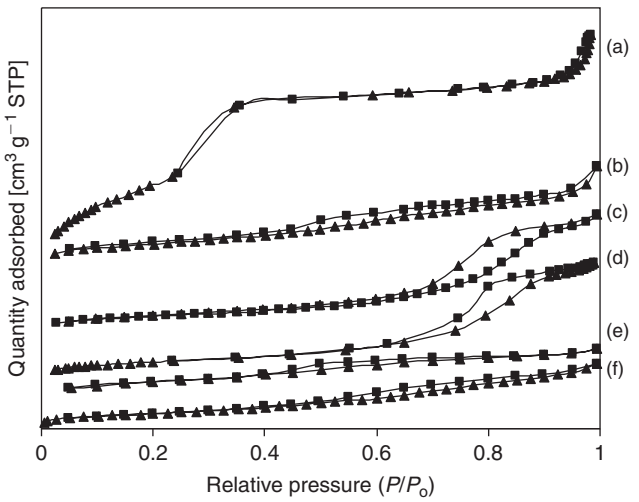

Fig. 3. Representative nitrogen adsorption-desorption isotherms of various silica based samples: (a) MCM-41; (b) GdSi_A; (c) GdSi_B; (d) GdSi_C; (e) GdSi_D and (f) GdSi_E samples. The isotherms for samples GdSi_D, GdSi_C, GdSi_B, GdSi_A and MCM-41 were vertically offset for clarity.

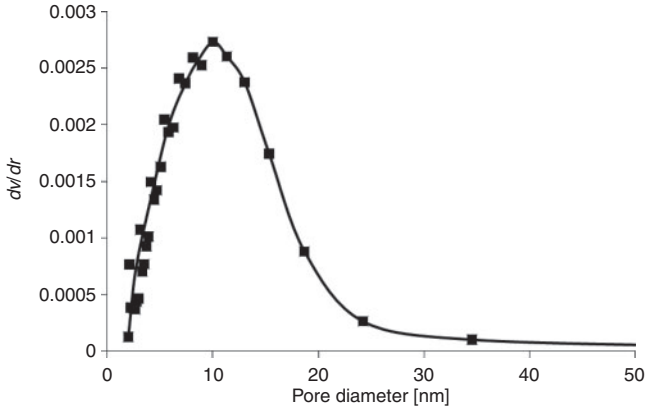

Fig. 4. Pore size distribution of a GdSi_B sample, calculated from the adsorption branch of the N_2 isotherm using the BJH equation. This distribution is typical for the sample series.

PSD for sample GdSi_B, Fig. 4, is very broad, spanning across ~25 nm in pore diameter. The span of pore sizes reflects the size distribution of the Gd oleate emulsion in solution. This range of pore sizes also suggests that the pores are disordered in packing, which is consistent with the XRD results. The typical BET surface areas for the various Gd oleate derived samples are in the range of 150–200 $m^2 g^{-1}$. This BET surface area is much lower than for the non-doped MCM-41 reference sample. This is to the disordered pore templating technique employed in this work. Additional contribution to the decreased surface area could also be due to the accessibility of the pores by the N_2 gas probe.[35]

The composition of the synthesized samples were analyzed by FT-IR, ^{29}Si MAS NMR and XPS. Fig. 5 shows spectra, acquired by FT-IR spectroscopy, in the range of 4000–400 cm^{-1} for the various synthesized samples with varying Gd loading. The major features of the FT-IR spectra for MCM-41 are peaks at 1224, 1066, 804 and 450 cm^{-1} (Fig. 5a). These peaks are characteristic of the network vibrational modes in a SiO_2 matrix. The 1224 and 1066 cm^{-1} bands are assigned to longitudinal optical (LO) and transversal optical (TO) Si–O–Si asymmetric stretching modes.[36] A broadening of the 1066 cm^{-1} band was associated with samples containing Gd. This is due to the occurrence of the unresolved 954 cm^{-1} band, which is often an indication of successful heteroatom incorporation into the silica matrix.[37] The bands at 804 and 450 cm^{-1} are associated with the stretching/vibration and bending of the Si–O–Si networks structure, respectively.[38] In addition, The lack of CH_2 vibration, indicated by the 2925 and 2852 cm^{-1} peaks,[39] in all the samples, except for possibly GdSi_B (Fig. 5c), suggests that the templating surfactants are completely removed during the calcination process.

XPS surface analysis of the samples was performed and indicated the existence of gadolinium ions in the silica matrix for the Gd doped samples. As expected, the two Gd $3d_{3/2}$ and Gd $3d_{5/2}$ peaks were observed only in the Gd doped samples (e.g. Fig. 6a). The silicon-to-oxygen (Si:O) ratio calculated from the XPS analysis in the reference sample, MCM-41, was a ratio of 1:2 consistent with SiO_2. The Si:O ratio for the Gd doped silica samples was lower, suggesting the existence of a gadolinium ion in the sample. Furthermore a shift of the O 1s peak (e.g. Fig. 6b) and the occurrence of Gd peaks indicated that gadolinium was successfully incorporated. Using MCM-41 as the reference, the nominal position of the O 1s peak was observed to be at 533.9 eV. In the Gd doped samples however, the position of the O 1s peak has been shifted to a lower energy of 532.78 eV.

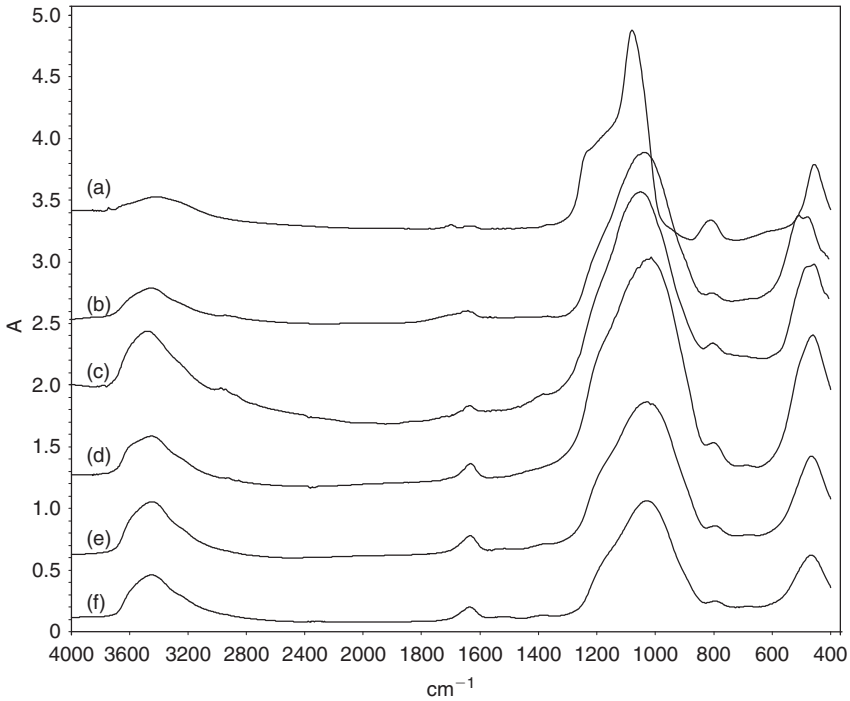

Fig. 5. FT-IR spectra of Gd loaded silica with different Gd loading (a) 0%; (b) 2.7%; (c) 8.8%; (d) 11.9%; (e) 14.6% and (f) 19.1%.

This is the result of the reduction of the effective positive charge of the Si^{4+} by the incorporated Gd^{III}.[40,41] In addition, the development of a shoulder peak at 530.66 eV was observed. This peak was assigned to be a Si–O–Gd bonding, which is consistent with literature reports.[28]

Solid state ^{29}Si MAS NMR spectrometry was also used as a complementary technique to confirm the presence of gadolinium in the silica matrix (e.g. Fig. 7). Three characteristic peaks were observed at −99.7, −102 and −109 ppm in MCM-41 (Fig. 7c) These peaks correspond to the $SiO_2(OH)_2$, $SiO_3(OH)$ and SiO_4 environments, respectively. The Q_4:Q_3:Q_2 ratio indicated that the samples are highly condensed and this value is in good agreement with literature reports.[36,42]

In the ^{29}Si MAS NMR spectra for the GdSi_C sample (Fig. 7b), a downfield shift of the native silica peaks along with peak broadening was also observed. This broadening is indicative of the presence of paramagnetic species.[43,44] The downfield shift of the silica peaks was attributed to the dipole interaction between the unpaired electrons and the silicon nucleus despite the absence of direct bonds. The hyperfine splitting of the peaks in the presence of the trivalent cation was not resolved at the particular sample rotor frequency, therefore the splitting was observed as a peak broadening effect. In addition, the decrease of the Q_2 and Q_3 peaks suggest that the silica bonding environment has changed. This is consistent with the formation of Gd–O–Si bonds and hence a decrease in the number of Si–O–Si bonds.[44–46]

The proton longitudinal and transverse relaxivities, r_1 and r_2 were determined at 20 MHz (representative plots are in Fig. 8a and Fig. 8b) and are summarized in Table 2 and Fig. 8c. The longitudinal relaxivity was observed to be consistent across the varying levels of doping, with a maximum observed value of 2.39 $mM^{-1}\,s^{-1}$ at 0.018 atomic fraction of incorporated gadolinium content. This is lower than the commercial standard MRI contrast agent Magnevist® with a r_1 value of 4.91 $mM^{-1}\,s^{-1}$. Factors that predominately affect the longitudinal relaxation

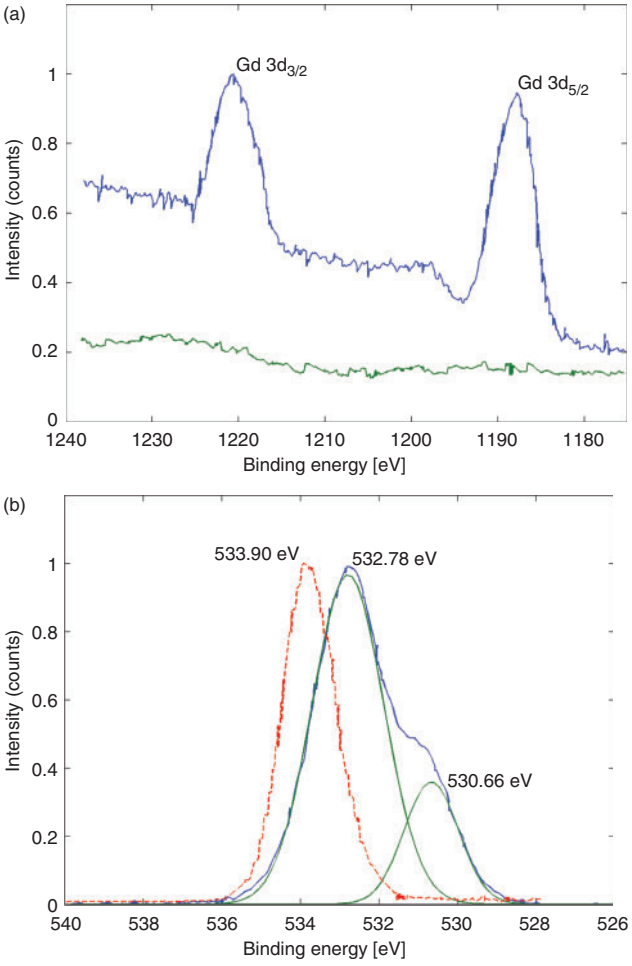

Fig. 6. (a) Gd 3d XPS spectrum of sample GdSi_C (top, blue) and MCM-41 sample (bottom, green); (b) O 1s XPS spectra MCM-41 (dotted line, red) and GdSi_C (solid line, blue) with its fitted peaks (green).

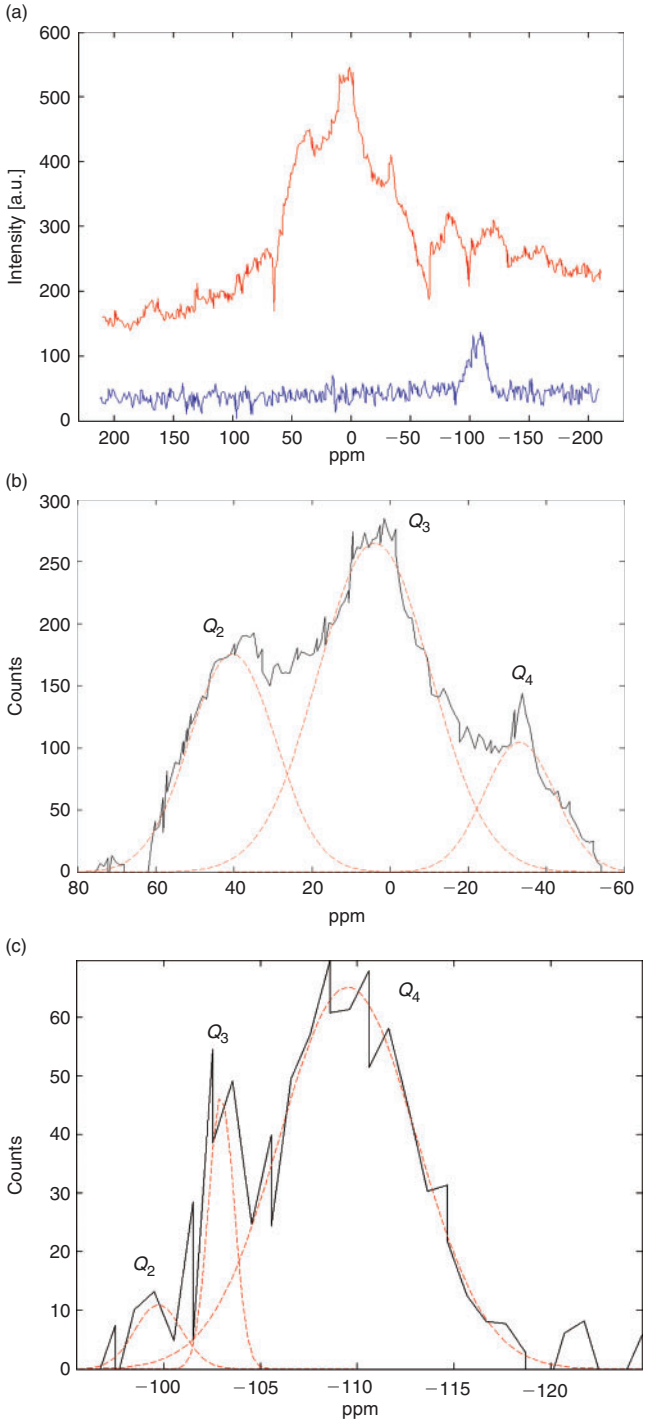

Fig. 7. ^{29}Si MAS NMR spectra: (a) raw spectra of the two measured samples; top trace GdSi_C and bottom trace MCM-41; (b) fitted spectra of the GdSi_C; (c) fitted spectra for MCM-41.

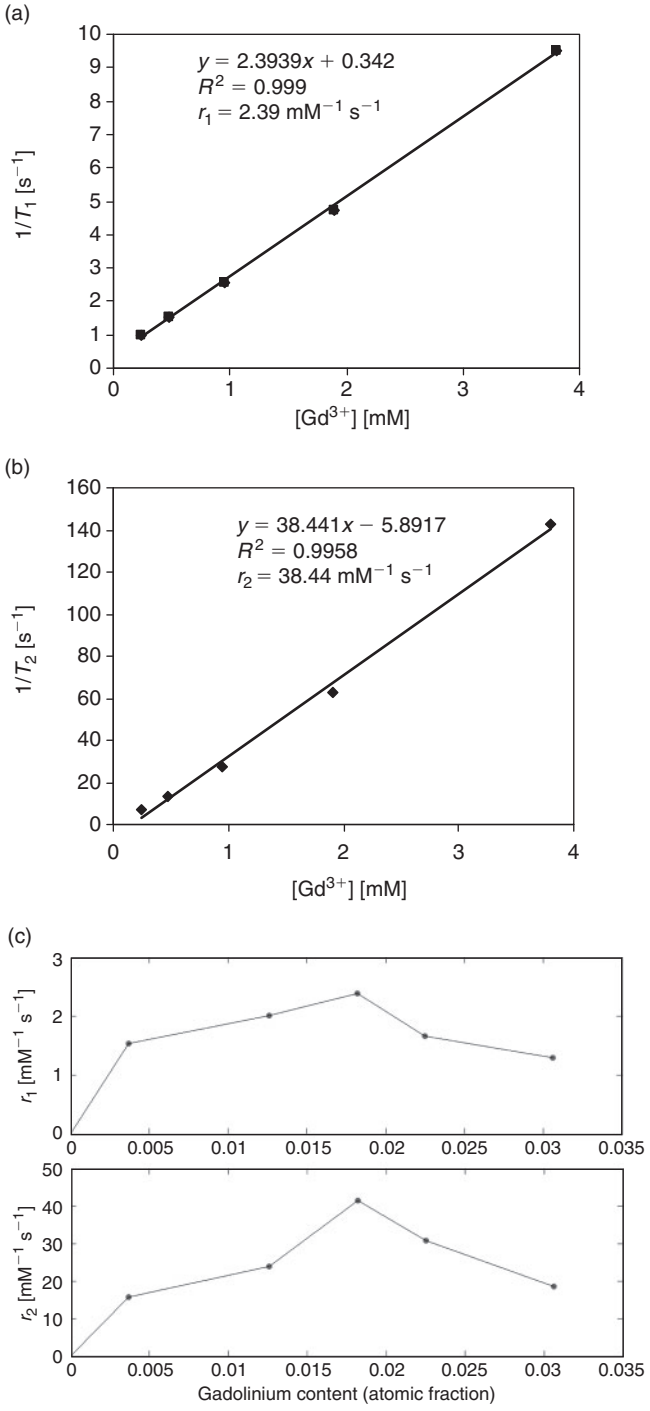

Fig. 8. The proton relaxivities determined at 20 MHz at room temperature GdSi_C. (a) example of r_1 determination for GdSi_C; (b) example of r_2 determination for GdSi_C and (c) r_1 (Top) and r_2 (Bottom) values for the various gadolinium doped silicate samples. Filled circles represent gadolinium doped sample data. Line is a visual guide.

include the number of bound water on the paramagnetic centre and the rate of diffusion of these waters in and around the paramagnetic centre. The seemingly low longitudinal relaxivity, despite the high gadolinium content, may be explained by reduced bound water within the coordination sphere of the gadolinium taken up in Gd-O bonds through their incorporation into the gadolinium-silicate framework,[21] in which case Magnevist® performs better solely due to the higher number of Gd-H_2O interactions per mole Gd. When comparing the relaxivity of the synthesized disordered-mesoporous material with an ordered porous silicate material such as the one reported by Lin et al., the ordered material outperforms the disordered.[28] This difference in longitudinal relaxivity is attributed to the difference in surface area between the disordered and ordered mesoporous materials, ~200 and 1000 $m^2\ g^{-1}$, respectively. The transverse relaxivity was also found to depend on the concentration of gadolinium content. The optimal doping level was also observed to be at 1.8 atomic percent gadolinium

Table 2. Relaxivities of different samples and commercial standard measured at 0.47 T (20 MHz) at 25°C

	ICP-AES Gd [wt%]	XPS Gd [at %]	XPS Gd [wt%]	r_1 [$mM^{-1} s^{-1}$]	r_2 [$mM^{-1} s^{-1}$]	r_2/r_1
Magnevist®	–	–	–	4.91	6.26	1.74
MCM-41	0.0	0.0	0.0	–	–	–
GdSi_A	2.7	0.4	3.0	1.54	15.77	10.24
GdSi_B	8.8	1.3	9.6	2.01	23.98	11.93
GdSi_C	11.9	1.8	13.1	2.39	41.52	17.37
GdSi_D	14.7	2.3	16.1	1.66	30.89	18.61
GdSi_E	19.1	3.0	20.9	1.29	18.64	14.45

doping. Further increase of gadolinium doping resulted in a decrease in transverse relaxivity. One factor that predominately affects the transverse relaxivity of a CA is the rotational correlation time of the paramagnetic centres in the agent. The observable improvement in the transverse relaxivity over Magnevist® has been suggested to be owing to the lengthening of rotational correlation time in the nanoparticulate CA.[47] The r_2 value for the GdSi_A sample is in fact comparable to the analogous Gd doped MCM-41 silicate sample (2.3% Gd-MS) reported by Lin et al. at the same magnetic field strength of 0.47 T.[28] Therefore the observed improvement in the transverse relaxivity is believed to be largely due to the reduced tumbling rate of the CA in solution. Further increase of gadolinium content results in a more homogeneous distribution of gadolinium throughout the silica matrix, resulting in further relaxivity improvement until the contribution of rotational effect reaches a maximum, 1.8 atomic percent gadolinium doping. At which point continual increase of gadolinium content results in a decrease of the measured relaxivity.[48,49] A similar saturation effect has also been observed in previous CA studies.[28,50–52] We continue to investigate the contribution of these physical parameters in affecting both the longitudinal and transverse relaxivity of these materials.

Conclusions

Gadolinium doped mesoporous silica (gadolinosilicate) nanoparticles have been successfully synthesized via the emulsified ionic liquid templating route. The silicate sample, with varying amount of gadolinium, was controlled by varying the amount of gadolinium oleate; acting as both the template agent and the gadolinium source. The synthesized samples were characterized in terms of particle size, structure and elemental composition by using SEM, XRD, nitrogen-gas sorption, FT-IR, XPS and ^{29}Si MAS NMR. The relaxivity of the final product was also measured and at low field strengths, it was found that the longitudinal relaxivity is comparable to the commercial standard Magnevist®. The transverse relaxivities reached an optimum value at 1.8 atomic percent gadolinium doping. This optimum relaxivity value is postulated to be the result of the reduced tumbling rate of Gd in the nanoparticulate construct. The results suggest that Gd doped porous silica nanoparticles have the potential to be used as MRI contrast agents. Further work is needed to elucidate the precise factors governing the observation of maximum relaxivity upon increased doping.

Acknowledgement

We thank Mr Mark Greaves for the SEM microscopy, Dr Thomas R. Gengenbach for help with running XPS samples, Dr Tim Bastow for the ^{29}Si MAS NMR characterization and the CSIRO Hierarchical Materials Emerging Science Initiative for financial support. G.L. and D.F.K. were the recipients of CSIRO postdoctoral fellowships, N.M.K.T. a CSIRO PhD studentship and C.J.D. an Australian Research Council Federation Fellowship during this work.

References

[1] M. Bottrill, L. Kwok, N. J. Long, *Chem. Soc. Rev.* **2006**, *35*, 557. doi:10.1039/B516376P
[2] S. Aime, C. Cabella, S. Colombatto, S. G. Crich, E. Gianolio, F. Maggioni, *J. Magn. Reson. Imaging* **2002**, *16*, 394. doi:10.1002/JMRI.10180
[3] S. Mansson, A. Bjornerud, *Physical principles of medical imaging by nuclear magnetic resonance* **2001** (John Wiley & Sons Ltd: Chichester).
[4] Q. A. Pankhurst, J. Connolly, S. K. Jones, J. Dobson, *J. Phys. D Appl. Phys.* **2003**, *36*, R167. doi:10.1088/0022-3727/36/13/201
[5] M. Liong, S. Angelos, E. Choi, K. Patel, J. F. Stoddart, J. I. Zink, *J. Mater. Chem.* **2009**, *19*, 6251. doi:10.1039/B902462J
[6] A. Louie, *Chem. Rev.* **2010**, *110*, 3146. doi:10.1021/CR9003538
[7] C. W. Lu, Y. Hung, J. K. Hsiao, M. Yao, T. H. Chung, Y. S. Lin, S. H. Wu, S. C. Hsu, H. M. Liu, C. Y. Mou, C. S. Yang, D. M. Huang, Y. C. Chen, *Nano Lett.* **2007**, *7*, 149. doi:10.1021/NL0624263
[8] H. B. Na, I. C. Song, T. Hyeon, *Adv. Mater. (Deerfield Beach Fla.)* **2009**, *21*, 2133. doi:10.1002/ADMA.200802366
[9] E. Tóth, L. Helm, A. E. Merbach, *Top. Curr. Chem.* **2002**, *221*, 61. doi:10.1007/3-540-45733-X_3
[10] J. H. Park, L. Gu, G. von Maltzahn, E. Ruoslahti, S. N. Bhatia, M. J. Sailor, *Nat. Mater.* **2009**, *8*, 331. doi:10.1038/NMAT2398
[11] N. Bloembergen, L. O. Morgan, *J. Chem. Phys.* **1961**, *34*, 842. doi:10.1063/1.1731684
[12] I. Solomon, *Phys. Rev.* **1955**, *99*, 559. doi:10.1103/PHYSREV.99.559
[13] P. Caravan, J. J. Ellison, T. J. McMurry, R. B. Lauffer, *Chem. Rev.* **1999**, *99*, 2293. doi:10.1021/CR980440X
[14] M. P. Lowe, *Aust. J. Chem.* **2002**, *55*, 551. doi:10.1071/CH02172
[15] T. J. Meade, A. K. Taylor, S. R. Bull, *Curr. Opin. Neurobiol.* **2003**, *13*, 597. doi:10.1016/J.CONB.2003.09.009
[16] H. Kato, Y. Kanazawa, M. Okumura, A. Taninaka, T. Yokawa, H. Shinohara, *J. Am. Chem. Soc.* **2003**, *125*, 4391. doi:10.1021/JA027555+
[17] B. Sitharaman, L. J. Wilson, *J. Biomed. Nanotechnol.* **2007**, *3*, 342. doi:10.1166/JBN.2007.043
[18] P. Caravan, *Chem. Soc. Rev.* **2006**, *35*, 512. doi:10.1039/B510982P
[19] H. B. Na, T. Hyeon, *J. Mater. Chem.* **2009**, *19*, 6233. doi:10.1039/B916598N
[20] A. J. L. Villaraza, A. Bumb, M. W. Brechbiel, *Chem. Rev.* **2010**, *110*, 2921. doi:10.1021/CR900232T
[21] V. Jacques, J. F. Desreux, *Top. Curr. Chem.* **2002**, *221*, 123. doi:10.1007/3-540-45733-X_5
[22] T. Grobner, *Nephrol. Dial. Transplant.* **2006**, *21*, 1104. doi:10.1093/NDT/GFK062
[23] D. R. Broome, M. S. Girguis, P. W. Baron, A. C. Cottrell, I. Kjellin, G. A. Kirk, *Am. J. Roentgenol.* **2007**, *188*, 586. doi:10.2214/AJR.06.1094
[24] P. Sharma, S. C. Brown, G. Walter, S. Santra, E. Scott, H. Ichikawa, Y. Fukumori, B. M. Moudgil, *Adv. Powder Technol* **2007**, *18*, 663. doi:10.1163/156855207782515030

[25] D. Zhao, J. Feng, Q. Huo, N. Melosh, G. H. Fredrickson, B. F. Chmelka, G. D. Stucky, *Science* **1998**, *279*, 548. doi:10.1126/SCIENCE.279.5350.548

[26] M. Vallet-Regi, A. Rámila, R. P. del Real, J. Pérez-Pariente, *Chem. Mater.* **2001**, *13*, 308. doi:10.1021/CM0011559

[27] L. Wang, W. J. Zhao, W. H. Tan, *Nano Res.* **2008**, *1*, 99. doi:10.1007/S12274-008-8018-3

[28] Y. S. Lin, Y. Hung, J. K. Su, R. Lee, C. Chang, M. L. Lin, C. Y. Mou, *J. Phys. Chem. B* **2004**, *108*, 15608. doi:10.1021/JP047829A

[29] G. Liu, C. E. Conn, C. J. Drummond, *J. Phys. Chem. B* **2009**, *113*, 15949. doi:10.1021/JP906344U

[30] Q. Cai, Z. S. Luo, W. Q. Pang, Y. W. Fan, X. H. Chen, F. Z. Cui, *Chem. Mater.* **2001**, *13*, 258. doi:10.1021/CM990661Z

[31] W. W. Lukens, P. Schmidt-Winkel, D. Y. Zhao, J. L. Feng, G. D. Stucky, *Langmuir* **1999**, *15*, 5403. doi:10.1021/LA990209U

[32] A. Derome, *Modern NMR techniques for chemistry research* **1987** (Pergamon Press: Oxford).

[33] A. Berggren, A. E. C. Palmqvist, K. Holmberg, *Soft Matter* **2005**, *1*, 219. doi:10.1039/B507551N

[34] J. Rouquerol, D. Avnir, C. W. Fairbridge, D. H. Everett, J. H. Haynes, N. Pernicone, J. D. F. Ramsay, K. S. W. Sing, K. K. Unger, *Pure Appl. Chem.* **1994**, *66*, 1739. doi:10.1351/PAC199466081739

[35] M. R. Hill, S. J. Pas, S. T. Mudie, D. F. Kennedy, A. J. Hill, *J. Mater. Chem.* **2009**, *19*, 2215. doi:10.1039/B817457A

[36] C. J. Brinker, G. W. Scherer, *Sol-gel science: the physics and chemistry of sol-gel processing* **1990** (Academic Press: San Diego).

[37] M. Selvaraj, B. H. Kim, T. G. Lee, *Chem. Lett.* **2005**, *34*, 1290. doi:10.1246/CL.2005.1290

[38] X. G. Zhao, J. L. Shi, B. Hu, L. X. Zhang, L. Z. Hua, *J. Mater. Chem.* **2003**, *13*, 399. doi:10.1039/B206732C

[39] J. M. Berquier, L. Teyssedre, C. Jacquiod, *J. Sol-Gel Sci. Technol.* **1998**, *13*, 739. doi:10.1023/A:1008609525830

[40] E. Rodríguez-Castellón, A. Jiménez-López, P. Maireles-Torres, D. J. Jones, J. Rozière, M. Trombetta, G. Busca, M. Lenarda, L. Storaro, *J. Solid State Chem.* **2003**, *175*, 159. doi:10.1016/S0022-4596(03)00218-4

[41] A. Y. Stakheev, E. S. Shpiro, J. Apijok, *J. Phys. Chem.* **1993**, *97*, 5668. doi:10.1021/J100123A034

[42] S. S. Kim, W. Zhang, T. J. Pinnavaia, *Science* **1998**, *282*, 1302. doi:10.1126/SCIENCE.282.5392.1302

[43] J. Plevert, T. Okubo, Y. Wada, M. O'Keeffe, T. Tatsumi, *Chem. Commun.* **2001**, *20*, 2112. doi:10.1039/B105881A

[44] W. Yin, M. Zhang, *J. Alloy. Comp.* **2003**, *360*, 231. doi:10.1016/S0925-8388(03)00304-9

[45] T. Asefa, M. J. MacLachlan, N. Coombs, G. A. Ozin, *Nature* **1999**, *402*, 867.

[46] Q. Huo, D. I. Margolese, U. Ciesla, P. Feng, T. E. Gier, P. Sieger, R. Leon, P. M. Petroff, F. Schuth, G. D. Stucky, *Nature* **1994**, *368*, 317. doi:10.1038/368317A0

[47] Z. P. Xu, N. D. Kurniawan, P. F. Bartlett, G. Q. Lu, *Chemistry* **2007**, *13*, 2824. doi:10.1002/CHEM.200600571

[48] R. A. Brooks, F. Moiny, P. Gillis, *Magn. Reson. Med.* **2001**, *45*, 1014. doi:10.1002/MRM.1135

[49] M. J. Gueron, *J. Magn. Reson.* **1975**, *19*, 58.

[50] G. Z. Liu, C. E. Conn, L. J. Waddington, S. T. Mudie, C. J. Drummond, *Langmuir* **2010**, *26*, 2383. doi:10.1021/LA902845J

[51] M. J. Moghaddam, L. de Campo, L. J. Waddington, C. J. Drummond, *Soft Matter* **2010**, *6*, 5915. doi:10.1039/C0SM00586J

[52] C. Platas-Iglesias, L. Vander Elst, W. Zhou, R. N. Muller, C. Geraldes, T. Maschmeyer, J. A. Peters, *Chemistry* **2002**, *8*, 5121. doi:10.1002/1521-3765(20021115)8:22<5121::AID-CHEM5121>3.0.CO;2-W